Title
CXC chemokine ligand 10 controls viral infection in the central nervous system: evidence for a role in innate immune response through recruitment and activation of natural killer cells.

Journal
Journal of virology, 78(2)

ISSN
0022-538X

Authors
Trifilo, Matthew J
Montalto-Morrison, Cynthia
Stiles, Linda N
et al.

Publication Date
2004

DOI
10.1128/jvi.78.2.585-594.2004

JOURNAL OF VIROLOGY, Jan. 2004, p. 585–594 Vol. 78, No. 2
0022-538X/04/$08.00+0 DOI: 10.1128/JVI.78.2.585–594.2004

CXC Chemokine Ligand 10 Controls Viral Infection in the Central Nervous System: Evidence for a Role in Innate Immune Response through Recruitment and Activation of Natural Killer Cells

Matthew J. Trifilo,[1] Cynthia Montalto-Morrison,[2] Linda N. Stiles,[1] Kelley R. Hurst,[2] Jenny L. Hardison,[1] Jerry E. Manning,[1] Paul S. Masters,[2] and Thomas E. Lane[1]*

Department of Molecular Biology and Biochemistry, University of California, Irvine, California 92697-3900,[1] *and Wadsworth Center, New York State Department of Health, Albany, New York 12201*[2]

Received 23 July 2003/Accepted 19 September 2003

How chemokines shape the immune response to viral infection of the central nervous system (CNS) has largely been considered within the context of recruitment and activation of antigen-specific lymphocytes. However, chemokines are expressed early following viral infection, suggesting an important role in coordinating innate immune responses. Herein, we evaluated the contributions of CXC chemokine ligand 10 (CXCL10) in promoting innate defense mechanisms following coronavirus infection of the CNS. Intracerebral infection of *RAG1*$^{-/-}$ mice with a recombinant CXCL10-expressing murine coronavirus (mouse hepatitis virus) resulted in protection from disease and increased survival that correlated with a significant increase in recruitment and activation of natural killer (NK) cells within the CNS. Accumulation of NK cells resulted in a reduction in viral titers that was dependent on gamma interferon secretion. These results indicate that CXCL10 expression plays a pivotal role in defense following coronavirus infection of the CNS by enhancing innate immune responses.

The CXC chemokine ligand 10 (CXCL10) is a non-ELR CXC chemokine that exerts a potent chemotactic effect on activated T cells through binding the receptor CXCR3 (5). CXCL10 is expressed within tissues following viral infection, suggesting an important role for this chemokine in host defense by contributing to lymphocyte activation, extravasation, and accumulation of virus-specific T cells within sites of infection. Indeed, recent studies with antibody-mediated targeting of CXCL10 and CXCL10$^{-/-}$ mice demonstrated that the absence of CXCL10 function results in increased mortality accompanied by increased viral titers and reduced T-cell infiltration within the brains of mice infected intracerebrally with a murine coronavirus (mouse hepatitis virus [MHV]) (8, 20). In addition, CXCL10 expression modulates the pathogenesis of liver disease in adenovirus-infected mice and transgenic mice capable of replicating hepatitis B virus by attracting CD8$^+$ T lymphocytes into the liver (2, 11).

These studies indicate that CXCL10 functions as a sentinel molecule in host defense and is important in the development of a protective T-cell response following viral infection. Recent findings have also illustrated an important role for chemokines in innate defense following viral infection. For example, in addition to its chemotactic effect on T cells, CXCL10 has also been shown to induce natural killer (NK) cell migration following viral infection (2, 11, 22, 23). Expression of both CXCL10 and CXC chemokine ligand 9 (CXCL9) has been found to contribute to antiviral immune responses in the absence of T and B cells (24). Although these chemokines have a demonstrated direct antimicrobial effect (6), their protective effect following vaccinia virus infection was a result of enhanced NK cell trafficking and activation (24).

Our laboratory is interested in the functional contributions of chemokines and chemokine receptors in both host defense and disease progression within the context of coronavirus infection of the central nervous system (CNS). Intracerebral infection of susceptible strains of mice with MHV results in an acute encephalomyelitis followed by a chronic immune-mediated demyelinating disease that is similar in pathology to the human demyelinating disease multiple sclerosis (16). A robust expression of chemokine genes occurs within the CNS following MHV infection that precedes and accompanies leukocyte entry (18).

Although NK cells can be readily detected within the CNS early following MHV infection, their precise contributions to antiviral immune responses within the CNS have not been well established. Furthermore, CXCL10 is prominently expressed as early as day 1 postinfection, suggesting that this molecule may function in enhancing innate immune responses by attracting NK cells into the CNS. Therefore, to further understand the relationship between CXCL10 and the innate immune response to viral infection of the CNS, we constructed a recombinant MHV capable of expressing mouse CXCL10. Intracerebral infection of *RAG1*$^{-/-}$ mice with this virus defines a pivotal role for CXCL10 in innate immunity to viral infection of the CNS by inducing the recruitment and activation of NK cells that results in reduced viral replication and enhanced survival. Moreover, our findings identify an important role for NK in controlling viral replication within the CNS prior to the development of an adaptive immune response.

* Corresponding author. Mailing address: Department of Molecular Biology and Biochemistry, 3205 McGaugh Hall, University of California, Irvine, CA 92697-3900. Phone: (949) 824-5878. Fax: (949) 824-8551. E-mail: tlane@uci.edu.

MATERIALS AND METHODS

Viruses and cells. All stocks of MHV-A59 mutants and recombinants were propagated in mouse 17 clone 1 (17Cl1) or DBT cells, and plaque titrations were

carried out with mouse L2 cells. For the determination of single-step growth kinetics, confluent monolayers of 17Cl1 cells (75 cm^2) were inoculated with Alb274 or Alb275 at a multiplicity of 2.5 PFU per cell for 2 h at 37°C with rocking every 15 min. Inocula were removed and replaced with medium, and incubation was continued at 37°C. Sample aliquots of medium were then withdrawn at 2, 4, 6, 8, 10, 12, and 24 h postinfection, and infectious titers were subsequently determined.

Plasmid constructs. A transcription vector for the construction of a CXCL10-expressing recombinant virus was derived from plasmid pMH54 (13). In brief, pMH54 contains the bacteriophage T7 RNA polymerase promoter and a cDNA copy of the 5′-most 0.5 kb of the MHV genome fused to the 3′-most 8.6 kb of the MHV genome. The MHV insert sequence exactly corresponds to that of wild-type MHV-A59, with the exception of coding-silent *Avr*II and *Ase*I sites introduced into the S protein open reading frame (ORF) and three nucleotide changes that create an *Sse*8387I site 12 bp downstream of the S ORF (13). This modification results in an upregulation of mRNA4 synthesis for reasons that are not currently understood.

Plasmid pCXCL10A was constructed from pMH54 in two steps (Fig. 1A). The CXCL10 ORF was amplified by PCR from plasmid pBS-CXCL-10 (generously provided by I. Campbell, Scripps Research Institute) with primers PM341 (5′-AGCC*CCTGCAGG*AAAGACAGAAAATCTAAACATC*ATG*AACCCAAGT GCTGC-3′; an *Sse*8387I site and the CXCL10 ORF start codon are italic) and PM342 (5′-G*TCTAGATTCCGGA*CAG*TTA*AGGAGCCCTTTTAGAC-3′; *Xba*I and *Bsp*EI sites and the complement of the CXCL10 ORF stop codon are italic). The resulting PCR product was restricted with *Pst*I and inserted in place of the *Sse*8387I-*Eco*RV segment of pMH54 to produce an intermediate construct, designated pCXCL10int. The *Sna*BI-*Nhe*I fragment of pMH54 was then restored in place of the blunted *Xba*I-*Nhe*I fragment of pCXCL10int to yield pCXCL10A (Fig. 1A). The compositions of all ligation junctions and the entire PCR-generated segment were confirmed by DNA sequencing. The resulting junction between the blunted *Xba*I site and the *Sna*BI remnant in pCXCL10A, which is 14 bp downstream of the end of the CXCL10 ORF (Fig. 1A), had a deletion of one base with respect to the predicted sequence.

Construction of MHV recombinants. CXCL10-expressing MHV recombinants and isogenic wild-type controls were constructed from the thermolabile N gene deletion mutant Alb4 by targeted RNA recombination, essentially as described previously (12, 26). Donor RNAs were transcribed from *Pac*I-truncated pCXCL10A or pMH54 with a T7 RNA polymerase kit (Ambion) and electroporated into Alb4-infected mouse L2 cells. Infected and transfected cells were then plated onto monolayers of mouse 17 clone 1 (17Cl1) cells, and virus was harvested from the supernatant medium following extensive syncytium formation in the monolayers. The Alb4 parental virus was counterselected by heat treatment at the nonpermissive temperature, and progeny recombinants that had restored the wild-type N gene were selected as viruses able to form large plaques at 39°C (12, 26).

Candidate recombinants were purified by two rounds of plaque titration on L2 cell monolayers, and three independent CXCL10 recombinants (Alb272 to Alb274) and a wild-type control (Alb275) were chosen for further analysis. Monolayers of 17Cl1 cells were infected with Alb272 to Alb275, and RNA was purified with Ultraspec reagent (Biotecx). The compositions of different genomic regions of each recombinant were confirmed directly by reverse transcription-PCR followed by restriction analysis or DNA sequencing. The primers (Fig. 1B) used for PCR were CK20 and FF35, flanking the CXCL10 insert and corresponding wild-type gene 4 region, respectively; PM119 and PM110, flanking the N gene deletion of Alb4; and FF29 and CK16, flanking the 5′ end of the S ORF.

Radiolabeling of viral RNA. Metabolic labeling of MHV-specific RNA in infected cells was carried out essentially as reported previously (26). In brief, monolayers of 17Cl1 cells in 20-cm^2 dishes were mock infected or infected with Alb274 or Alb275 at a multiplicity of 10 PFU per cell and incubated at 37°C. When infections had progressed to the extent of approximately 50% syncytium development (at about 5.5 h), cells were starved for phosphate for 2 h and then labeled for 2 h in phosphate-free medium containing 100 μCi of [^{33}P]orthophosphate (ICN) per ml, 5% dialyzed fetal bovine serum, and 20 μg of actinomycin D (Sigma) per ml. Total cytoplasmic RNA was purified by a gentle NP-40 lysis procedure. RNA samples containing equal amounts of radioactivity (or an RNA sample from an equivalent number of mock-infected cells) were denatured with formaldehyde and formamide, analyzed by electrophoresis through 1% agarose-containing formaldehyde, and visualized by fluorography.

Western blotting and immunofluorescence. For Western blotting, confluent 20-cm^2 monolayers of 17Cl1 cells were infected with Alb274 or Alb275 at a multiplicity of 0.25 PFU/cell or else mock infected and incubated at 33°C. At 19 h postinfection, monolayers were washed twice with phosphate-buffered saline (PBS) and lysed with 500 μl of interferon-inducible buffer (50 mM Tris-HCl, pH 8.0, 150 mM NaCl, 1.0% Nonidet P-40, 0.7 μg of pepstatin per ml, 1.0 μg of leupeptin per ml, 1.0 μg of aprotinin per ml, 0.5 mg of Pefabloc SC per ml) for 15 min at 4°C. Lysates were clarified by centrifugation, and 10-μl samples of each were separated by sodium dodecyl sulfate-polyacrylamide gel electrophoresis (SDS-PAGE) on 15% polyacrylamide, transferred to a polyvinylidene difluoride membrane, and probed with rabbit antiserum specific for CXCL10 (PeproTech) or with rabbit antiserum raised against a bacterially expressed maltose-binding protein-MHV N fusion protein. Bound antibodies were visualized with a chemiluminescent detection system (ECL; Amersham).

For immunofluorescence assays, L2 cells grown in 4.2-cm^2 wells on glass slides were infected with Alb274 or Alb275 at a multiplicity of 5 PFU/cell or else mock infected and incubated at 37°C. At 6 h postinfection, cells were fixed with 2% paraformaldehyde in PBS, blocked in PBS containing 100 mM glycine, and permeabilized with 50% acetone–50% methanol at −20°C. Cells were blocked in PBS containing 0.2% Tween 20, 3% immunoglobulin G-free bovine serum albumin, and 3% normal goat serum prior to incubation with anti-CXCL10 or anti-MHV N primary antibodies. Cells were then washed with PBS containing 0.2% Tween 20, incubated with goat anti-rabbit immunoglobulin G $F(ab')_2$ fluorescein isothiocyanate-conjugated secondary antibody (Roche), and counterstained with 0.01% Evans blue. Specimens were viewed on an Axioskop fluorescence microscope fitted with Zeiss filter set 10 and photographed with Kodak Tmax 400 film.

Animals. C57BL/6 and *RAG1*$^{-/-}$ mice (*H-2*^{b} background) were purchased from Jackson Laboratory (Bar Harbor, Maine), and *CCL3*$^{-/-}$ mice were generated previously (C57BL/6, *H-2*^{b}) (7). Mice were anesthetized by inhalation of methoxyflurane (Pitman-Moore Inc., Washington Crossing, N.J.) and injected intracerebrally with 5,000 PFU of either Alb274 or Alb275 suspended in 30 μl of sterile PBS. Control mice were injected with 30 μl of sterile PBS alone.

Antibody preparation and treatment of mice. To neutralize functional CXCL10 in vivo, a monoclonal antibody was developed against murine CXCL10. Hybridoma cell lines producing monoclonal antibody against CXCL10 were created by immunizing BALB/c mice with a peptide corresponding to an epitope of CXCL10 (CIHIDDGPVRMRAIGK) previously shown to produce neutralizing antibodies to CXCL10 (19, 20). Spleens from immunized mice were removed and fused with SP2/0 myeloma cells. Hybridoma cell lines that produced antibodies against CXCL10 were selected by enzyme-linked immunosorbent assay (ELISA) and cloned twice by limiting dilution. Clone IP6C7 was chosen and purified from culture supernatant by affinity chromatography on Sepharose-protein G columns and filter sterilized for use in vivo. IP6C7 showed reactivity to recombinant mouse CXCL10 (CXCL10; Pharmingen, San Diego, Calif.) to a dilution of >1:500,000 via ELISA. Clone IP6C7 showed no cross-reactivity for non-ELR CXC chemokines. The ability to bind and neutralize CXCL10 function was determined by the inhibition of in vitro chemotaxis and Ca^{2+} flux with a cell line transfected with CXCR3 (kindly provided by B. Moser) in response to recombinant mouse CXCL10 (22) (data not shown). Clone IP6C7 also blocked the accumulation of T cells in the CNS of mice following intracerebral infection with MHV (data not shown).

Rabbit monoclonal anti-IFN-γ (clone XMG1.6) was purchased from BD Pharmingen. Mice were injected with 0.5 ml of anti-CXCL10 (≈0.5 mg/ml) or 0.2 ml of anti-NK1.1 (≈1.1 mg/ml) on days −1, 0, 1, and 3 postinfection and sacrificed at days 2 and 5 postinfection. Mice injected intraperitoneally with anti-IFN-γ (0.25 mg/ml, days 3 and 6 postinfection) were sacrificed on day 8 postinfection. Rabbit antiserum specific to NK1.1 has been described previously and effectively removes natural killer cells from mice (34).

Mononuclear cell isolation and flow cytometry. Mononuclear cells were obtained from the brains of mice by centrifugation through a discontinuous Percoll gradient as previously described (17). Cell surface expression following MHV infection was examined with fluorescein isothiocyanate-conjugated rat anti-mouse NK1.1. Data are presented as the mean ± standard error of the mean. Data are presented as the percentage of positive cells within the gated population. The absolute numbers of NK1.1-positive cells was calculated by multiplying the fraction of positive cells by the total number of cells obtained from the brain.

IFN-γ and CXCL10 ELISA. IFN-γ was quantified in brain samples obtained from either Alb274- or Alb275-infected mice with the Quantikine M mouse IFN-γ immunoassay kit (R & D Systems, Minneapolis, Minn.) with a previously described method (17). The results are presented in picograms per milliliter. The limit of sensitivity of IFN-γ detection was approximately 9.4 pg/ml. Assessment of CXCL10 in the supernatants of Alb274- and Alb275-infected cells was determined with a noncommercial ELISA. The detection limit for CXCL10 was 312.5 pg/ml.

RNase protection assay. Chemokine gene expression was determined with the multitemplate probe set mCK-5 (Pharmingen, San Diego, Calif.) with a previously described protocol (17). CXCL9 and CXCL10 transcripts were detected

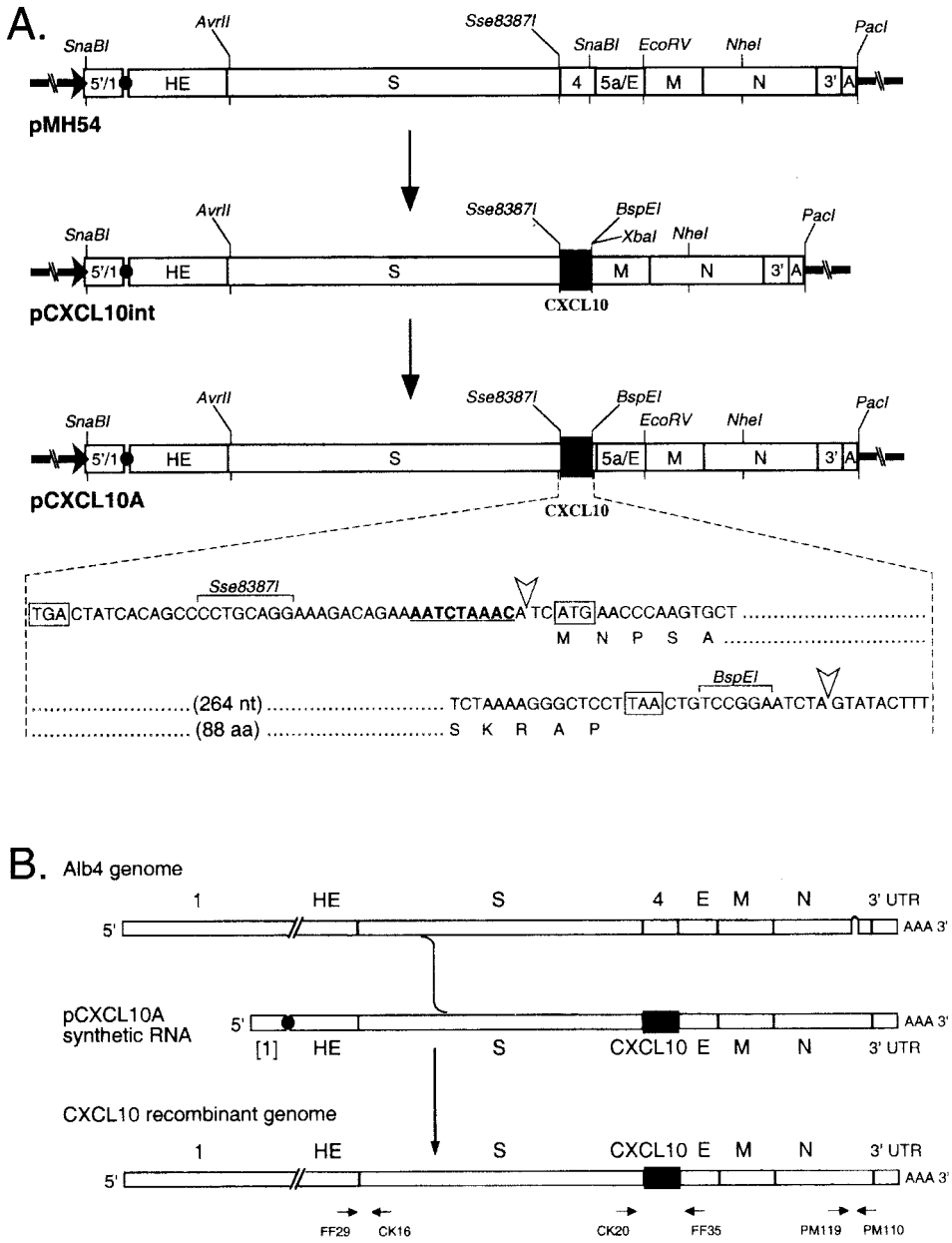

FIG. 1. Construction of a CXCL10-expressing recombinant of MHV-A59. (A) Construction of a transcription vector for synthesis of donor RNA. Plasmid pCXCL10A was derived in two steps from parent plasmid pMH54 via an intermediate construct, pCXCL10int; the net change was the removal of 267 nucleotides of MHV sequence from pMH54 and its replacement with 313 nucleotides of CXCL10 sequence in pCXCL10A. Restriction sites shown are those relevant to plasmid construction, runoff in vitro transcription, or recombinant analysis. The expanded region of sequence shows the context of the inserted CXCL10 ORF. The start and stop codons of the CXCL10 ORF and the stop codon of the upstream S ORF are boxed. The gene 4 transcription regulating sequence is underlined. Arrowheads mark the boundaries between MHV sequence and the CXCL10 insert. (B) Scheme for generation of MHV-A59 CXCL10 recombinants by targeted recombination between the parental virus, thermolabile N gene deletion mutant Alb4, and donor RNA transcribed from plasmid pCXCL10A. A single crossover upstream of the gene 4 region generated recombinants that had simultaneously acquired the CXCL10 insertion and the wild-type copy of the N gene. The same strategy, with donor RNA transcribed from pMH54, was used to generate an isogenic wild-type control recombinant. At the bottom are shown the primer pairs used in reverse transcription-PCR analysis of recombinant viral genomes.

with previously described antisense riboprobes (20). Target samples represented total RNA (15 μg) obtained from the brains of mice infected with either Alb274 or Alb275 at defined times postinstillation of either virus. For quantification of signal intensity, autoradiographs were scanned and individual chemokine transcript signals were normalized as the ratio of band intensity to the internal L32 control present within each probe set. Analysis was performed with NIH Image 1.61 software (19).

Statistical analysis. All data were analyzed by performing Student's *t* test with Sigma-Stat 2.0 software. Values of P of ≤ 0.05 were considered significant.

RESULTS

Construction of a recombinant of MHV expressing CXCL10. In order to assess the functional contributions of

CXCL10 in promoting innate immune responses within the CNS following viral infection, we constructed a recombinant of MHV capable of expressing CXCL10 with the goal of instilling this virus into the CNS of *RAG1*$^{-/-}$ mice and evaluating disease severity. We chose to insert the exogenous CXCL10 gene into a functional transcription unit in the genome of MHV-A59 in place of most of gene 4. MHV gene 4 encodes a nonstructural protein that is not essential either in tissue culture or in the mouse host (28, 36, 38). This has been most clearly shown in the JHM strain of MHV, where targeted disruption of both transcription and translation of gene 4 was demonstrated to have no detectable effect on growth in tissue culture or virulence in the mouse CNS (28). Moreover, in MHV-A59 the expression of gene 4 is abolished by a frameshift mutation that truncates the protein after 19 codons (36).

The CXCL10-expressing recombinant of MHV was generated by targeted RNA recombination, a reverse genetic system that has been used to manipulate the 31-kb RNA genome of MHV (12, 13, 25, 26). To construct recombinants, the CXCL10 ORF was first introduced, in two steps, into plasmid pMH54 downstream of the gene 4 transcription-regulating sequence and replacing the first two-thirds of gene 4 (Fig. 1A). In the final transcription vector, pCXCL10A, this resulted in the removal of 267 nucleotides of MHV sequence and its replacement by 313 nucleotides of CXCL10 sequence. This alteration was then incorporated into MHV through RNA-RNA recombination between pCXCL10A-derived synthetic transcripts and the genome of the N gene deletion mutant Alb4 (Fig. 1B), which was selected against on the basis of its thermolability (12, 25). An isogenic wild-type control, constructed with pMH54 donor RNA, was generated in the same manner.

Independent, plaque-purified CXCL10 recombinant candidates were characterized by reverse transcription-PCR analysis of viral RNA, and the integrity of the CXCL10 ORF (or the wild-type gene 4 in the control) and its upstream transcription-regulating sequence was ascertained by direct sequencing of purified PCR products. One CXCL10 recombinant virus, Alb274, and its matched wild-type control, Alb275, were chosen for subsequent experiments with mice.

In vitro phenotype of the CXCL10 recombinant. Both Alb274 and Alb275 formed plaques indistinguishable in size and morphology in tissue culture, and both viruses grew to high titers, producing comparable numbers of syncytia and degrees of cytopathic effect in infected cells. To directly compare the two recombinants, we infected monolayers at a multiplicity of 2.5 PFU per cell and determined the infectious titer of virus released at various times from 2 to 24 h postinfection This revealed that the growth kinetics of the CXCL10 recombinant and its wild-type counterpart were indistinguishable (Fig. 2A).

We next examined RNA synthesis in cells infected by Alb274 and Alb275. Coronavirus gene expression entails the transcription of a 3′ nested set of subgenomic RNAs (sgRNAs), each of which acts as the functionally monocistronic mRNA for its 5′-most ORF (14). To selectively metabolically label viral RNA, infected cells that had been starved for phosphate were incubated with [^{33}P]orthophosphate in the presence of actinomycin D, which inhibits cellular transcription, and purified RNA was then analyzed by electrophoresis. As seen in Fig. 2B, the transcription patterns observed for Alb274 and Alb275 were nearly identical. In particular, sgRNA4 of Alb274, the mRNA from which CXCL10 is expressed, was synthesized at a level comparable to that of wild-type sgRNA4 of Alb275. A faint extra band, of slightly higher mobility than that of sgRNA4, was observed in the Alb274 samples. This most likely arose from aberrant transcription, as has previously been observed with the insertion of heterologous genetic material into the MHV genome (9), but it constituted a very minor species by comparison with full-length sgRNA4. Additionally, the transcription analysis showed that the insertion of the CXCL10 gene into Alb274 did not somehow alter the expression of other viral sgRNAs, many of which encode essential viral structural proteins.

To ascertain whether CXCL10 was truly expressed by the engineered recombinant virus, cell lysates from mock-infected cells or from cells infected with Alb274 or Alb275 were analyzed by Western blotting. Antibodies specific for CXCL10 detected a band consistent with the calculated molecular mass of 8.7 kDa for mature CXCL10 protein only in the lysate from Alb274-infected cells and not in lysates from Alb275- or mock-infected cells (Fig. 2C). Control antibodies specific for the MHV nucleocapsid (N) protein, as expected, detected equivalent amounts of N protein in both Alb274- and Alb275-infected cell lysates. Next, the temporal production of CXCL10 secreted into the extracellular medium was assessed following infection of the cell culture with Alb274 and Alb275. The results shown in Fig. 2D demonstrate increased expression of CXCL10 protein at 2, 4, and 8 h postinfection compared to cells infected with Alb275. Expression of CXCL10 was also demonstrated by immunofluorescence analysis (Fig. 3). Cells infected with either Alb274 or Alb275 exhibited a relatively uniform cytoplasmic pattern of immunofluorescence in single cells and in syncytia probed with antibody against the MHV N protein (Fig. 3F and I). By contrast, anti-CXCL10 antibodies revealed a punctate pattern of staining, consistent with localization to the endoplasmic reticulum, only in cells infected with Alb274 (Fig. 3E).

Intracerebral infection of *RAG1*$^{-/-}$ mice. In order to determine if CXCL10 contributed to enhancing nonspecific antiviral immunity, *RAG1*$^{-/-}$ mice were infected with 5,000 PFU of either Alb274 or Alb275 and mortality was assessed. As shown in Fig. 4A, intracerebral infection with Alb275 resulted in death as early as 3 days postinfection and 100% mortality by day 10 postinfection. In contrast, Alb274-infected mice displayed 100% survival as long as 10 days following infection. However, Alb274-infected mice did eventually succumb (100% mortality) by day 14 postinfection, indicating that death is delayed, not prevented, by increasing CXL10 expression within the CNS (Fig. 4A). The rapid mortality observed following Alb275 infection was associated with severe morbidity. However, Alb274-infected mice displayed only muted clinical signs of disease and never reached the morbidity levels observed in Alb275-infected mice (data not shown).

We next determined viral titers within the brains of mice infected with either Alb274 or Alb275. Correlating with the reduced mortality, infection with Alb274 resulted in a dramatic reduction in recovery of virus from brains at days 2, 5, and 8 postinfection compared to Alb275-infected mice (Table 1). Analysis of surviving mice at day 8 postinfection revealed that Alb274-infected mice retained an approximately 2-log (10) reduction in viral titers. However, by day 12 postinfection, viral

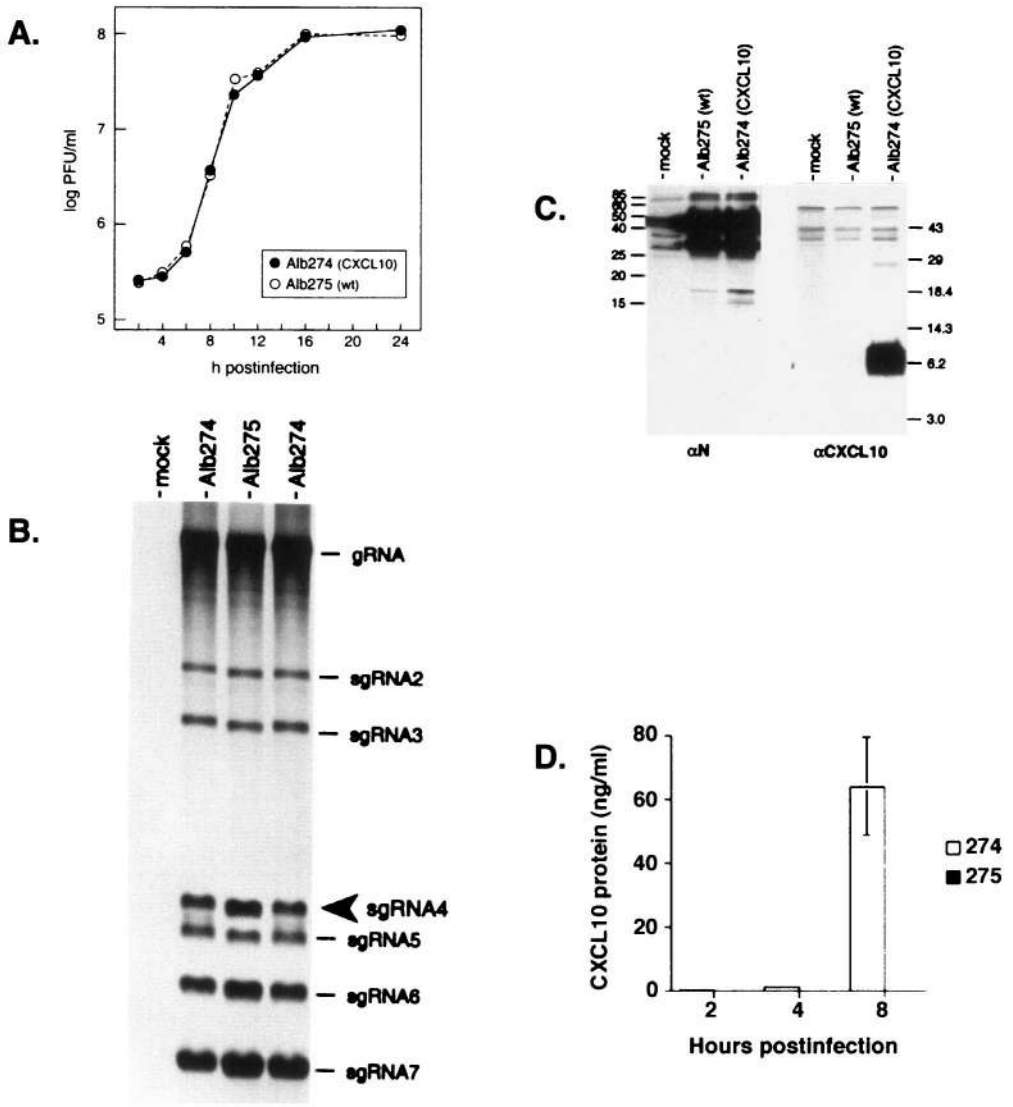

FIG. 2. (A) Single-step growth kinetics of the CXCL10-expressing recombinant and isogenic wild-type MHV. Confluent monolayers of 17Cl1 cells were infected with Alb274 and Alb275 at a multiplicity of 2.5 PFU per cell. At the indicated times postinfection, aliquots of medium were removed and plaque titers were determined on mouse L2 cells. A duplicate of the experiment shown gave virtually the same results. (B) Analysis of virus-specific RNA synthesis in infected cells. Mouse 17Cl1 cells were mock infected or infected with the CXCL10 recombinant (Alb274) or its reconstructed wild-type counterpart (Alb275) and then labeled from 7.5 to 9.5 h postinfection with [^{33}P]orthophosphate in the presence of actinomycin D. Purified total cytoplasmic RNA was separated by electrophoresis through 1% agarose-containing formaldehyde, and labeled RNA was visualized by fluorography. The mobility of sgRNA4, the mRNA for CXCL10 in Alb274, is indicated by an arrowhead. The sizes of the RNA species are 31.5 kb for genomic (g) RNA and 9.9, 7.7, 3.7, 3.3, 2.6, and 1.9 kb for sgRNAs 2 through 7, respectively. (C) Western blot analysis of protein expression in infected cells. Samples of lysates from mock-, Alb275-, and Alb274-infected cells were separated by SDS-PAGE, transferred to a polyvinylidene difluoride filter, and probed with antibodies to CXCL10 (right panel) or to the MHV N protein (left panel). Molecular masses (in kilodaltons) of marker proteins are indicated. N protein appears as a doublet owing to a significant amount of intracellular proteolysis of this highly basic protein. (D) ELISA analysis of CXCL10 protein expression from the supernatants of infected cells. Samples of supernatants from Alb274- and Alb275-infected cells were collected at 2, 4, and 8 h postinfection CXCL10 protein was detectable following Alb274 infection by 2 h postinfection and most prominently at 8 h postinfection.

titers within the CNS of Alb274-infected mice had increased to the levels that had been observed in Alb275-infected mice at days 5 and 8, and this correlated with the onset of mortality (Table 1).

NK cell infiltration and IFN-γ production in infected mice. CXCL10 has previously been shown to be chemotactic for T lymphocytes and NK cells expressing CXCR3 (2, 11, 20, 22). To determine if the decrease in mortality and viral burden reflected differences in the profile of NK cell infiltration, flow cytometric analysis of mononuclear cells isolated from the CNS of Alb274- and Alb275-infected mice was performed. The results shown in Table 1 and Fig. 5A and B reveal that Alb275 infection of *RAG1*$^{-/-}$ mice resulted in NK cell recruitment within 2 days postinfection However, NK cell infiltration was

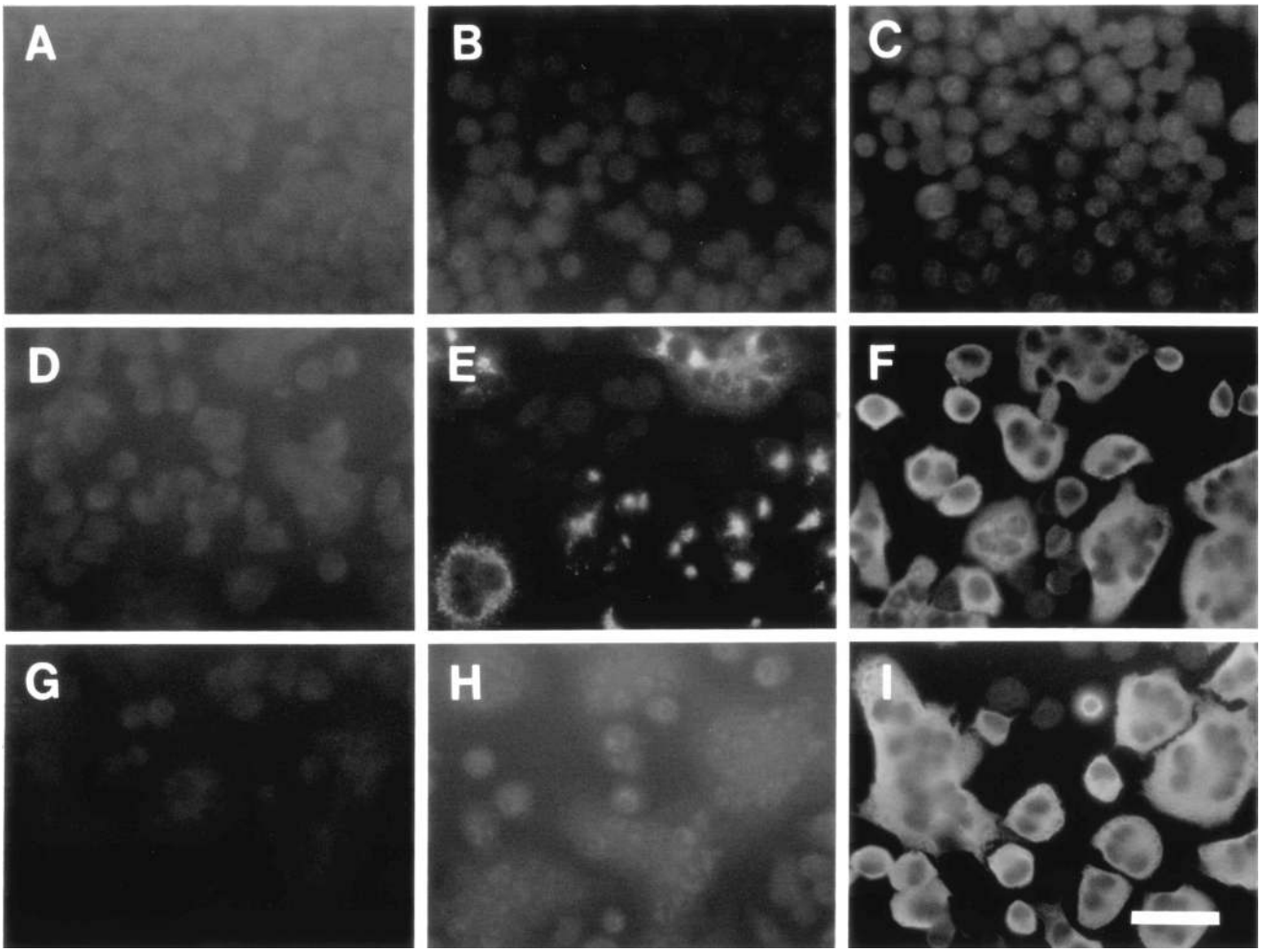

FIG. 3. Detection of protein expression in infected cells. Mouse L2 cells were mock-infected (A, B, and C), or infected with Alb274 (D, E, and F) or Alb275 (G, H, and I). After 6 h of incubation, cells were fixed and analyzed by immunofluorescence with antibodies to CXCL10 (B, E, and H) or to MHV N protein (C, F, and I) or phosphate-buffered saline as a control (A, D, and G), followed by fluorescein isothiocyanate-conjugated goat anti-rabbit antibody. Bar, 50 μm.

dramatically decreased by day 5 postinfection. Interestingly, NK cell recruitment was significantly increased ($P \leq 0.0001$) at day 2 postinfection following Alb274 infection compared to Alb275-infected mice (≈2-fold increase) and remained elevated (≈5-fold increase) at day 5 compared to Alb275-infected mice. However, the level of NK infiltration was substantially reduced by day 8 postinfection within the CNS of Alb274-infected mice compared to day 5 postinfection, which correlated with the increased mortality observed.

In order to determine the contributions of NK cells to host defense against MHV infection of the CNS, Alb274-infected mice were treated with neutralizing anti-NK antiserum and disease was assessed. Analysis of cellular infiltration within the CNS indicated that anti-NK treatment resulted in 98% and 97% reduction in NK cell infiltration compared to Alb274-infected mice at days 2 and 5, respectively. The absence of NK cells within the CNS resulted in a marked increase in viral titers at both 2 and 5 days postinfection (≥ 1 $\log_{10}$ increase), indicating that NK cells are important in controlling viral replication in infected *RAG1*$^{-/-}$ mice (Table 1).

One mechanism by which NK cells can participate in host defense against viral infection is through the secretion of antiviral cytokines such as IFN-γ. Indeed, IFN-γ has previously been shown to exert a potent antiviral effect on MHV replication within the CNS (15, 30). Therefore, levels of IFN-γ protein were measured within the brains of Alb274- and Alb275-infected mice at day 5 postinfection. As shown in Fig. 4B, there was an approximately twofold increase in IFN-γ production within the brains of Alb274-infected mice compared to Alb275-infected mice that correlated with the pronounced increase in NK cells present in the CNS of these mice at this time. To further examine the contributions of IFN-γ to the protective effects of infiltrating NK cells, Alb274-infected mice were treated with a neutralizing anti-IFN-γ antibody at days 4 and 6 postinfection. Neutralization of IFN-γ resulted in an increase in both mortality and viral titers compared to Alb274-infected mice (Table 1). In addition, a 50% reduction in the frequency of infiltrating NK cells present within the CNS of anti-IFN-γ-treated mice was observed. These data suggest that IFN-γ is critical in NK-mediated control of viral replication

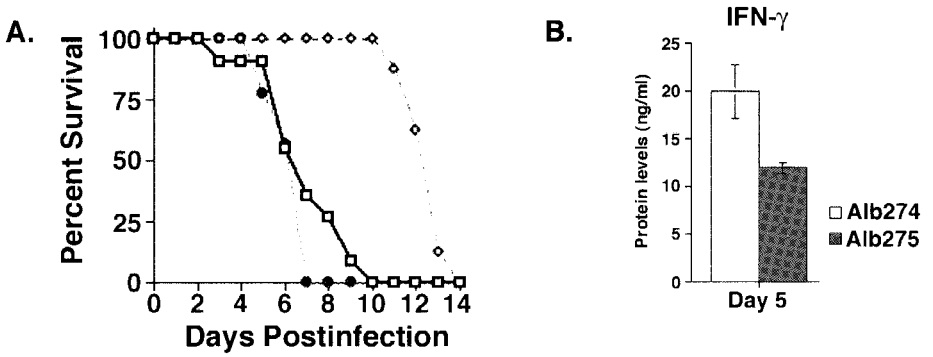

FIG. 4. (A) Decreased rate of mortality of Alb274-infected mice. *RAG1*$^{-/-}$ mice were infected intracerebrally with 5,000 PFU of either Alb274 or Alb275 and treated with neutralizing anti-CXCL10 antibodies. Alb275-infected mice (represented by solid line with open squares) exhibited 100% mortality by 10 days postinfection. In contrast, mortality was not observed in Alb274-infected mice (represented by dashed line with open diamonds) until day 11 postinfection. However, Alb274 infection eventually resulted in death of all mice by day 14 postinfection, indicating that death was delayed by CXCL10 expression. Data presented represent a total of three separate experiments with at least three mice per group; $n = 9$. Anti-CXCL10 treatment of Alb274-infected mice (represented by dotted line with solid circles) resulted in rapid mortality, and 100% of treated animals died by day 7 postinfection. Data presented for anti-CXCL10 treatment represent a total of three separate experiments with three mice per group; $n = 9$. (B) IFN-γ protein levels within the CNS. Protein levels isolated from the CNS were determined by ELISA at 5 days postinfection. Alb274-infected mice displayed significantly increased levels of IFN-γ compared to Alb275-infected mice at day 5 postinfection ($P \leq 0.05$). The data shown represent two separate experiments with three mice per experiment, $n = 6$.

within the CNS following MHV infection. In addition, IFN-γ may also support NK infiltration and/or survival.

Antibody-mediated depletion of CXCL10. Instillation of Alb274 into the CNS of *RAG1*$^{-/-}$ mice resulted in increased transcripts levels for CXCL10 but not CXCL9 compared to Alb275-infected mice (data not shown). To determine whether NK cell infiltration was directly mediated by CXCL10 expression, mice were treated with a mouse monoclonal anti-CXCL10 neutralizing antibody, and survival, cellular infiltration into the CNS, and viral clearance were assessed. Neutralization of CXCL10 following Alb274 infection resulted in a striking increase in mortality that correlated with increased viral titers within the brains at both days 2 and 5 postinfection compared to untreated mice (Fig. 4A and Table 1). CXCL10-mediated defense directly correlated with the ability to recruit NK cells, as neutralization of CXCL10 also resulted in significant reduction in NK cell infiltration at both 2 and 5 days postinfection (Table 1; Fig. 5E and F). Anti-CXCL10 treatment following Alb275 infection also resulted in enhanced viral recovery and reduced NK cell infiltration at days 2 and 5 postinfection, indicating that CXCL10 production following infection with wild-type virus also contributes to NK cell entry and host defense (Table 1; Fig. 5C and D).

CCL3 does not contribute to NK accumulation within the brains of MHV-infected mice. The results presented above indicate that CXCL10-mediated recruitment of NK cells was the primary effector mechanism responsible for reducing viral replication in the absence of T cells. However, there remained the possibility that CXCL10 expression in Alb274-infected mice was contributing to NK cell recruitment indirectly through inducing additional chemokines that may also exert a chemotactic effect on NK cells. Indeed, CCL3 can directly participate in the recruitment of NK cells into the liver following murine cytomegalovirus infection (33).

To address this issue, we analyzed *CCL3* mRNA expression within the CNS of Alb274- and Alb275-infected mice at 2 and 5 days postinfection. Intracerebral infection with either Alb274 or Alb275 viruses resulted in increased transcript levels for *CCL3*. Alb274 infection resulted in a significant increase in *CCL3* mRNA levels at day 2 postinfection compared to those in Alb275-infected mice (Fig. 6A). In order to determine whether CCL3 was contributing to NK cell recruitment within the CNS of infected mice, mice lacking CCL3 (*CCL3*$^{-/-}$) were infected intracerebrally with Alb274, and NK cell infiltration was determined at day 2 postinfection. No difference in NK cell recruitment was detected compared to wild-type C57BL/6 mice infected with Alb274, indicating that CCL3 expression was not necessary for the recruitment of NK cells into the CNS following MHV infection (Fig. 6B). Furthermore, there were no differences in viral titers within the CNS of Alb274-infected *CCL3*$^{-/-}$ and *CCL3*$^{+/+}$ mice (Fig. 6B).

DISCUSSION

Recent studies have used various genetic methods for assessing the contributions of both cellular and viral genes to host defense and disease in various models, including tumor biology and viral pathogenesis. Protection from infection and abnormal cellular growth is dependent upon the combined activation and recruitment of NK cells, macrophages, and T lymphocytes to the site of infection. Recently, recombinant viruses have been used to further characterize the molecules required for controlling the amplitude and type of immune response elicited following infection and tumor growth. For example, the course of vaccinia virus infection can be biased toward a protective antiviral response through coexpression of type 1 cytokines, whereas delivery of type 2 cytokines results in immunosuppression and enhanced susceptibility to virally induced disease (10, 32). Furthermore, adenovirus delivery of proinflammatory cytokines enhances antitumor immune responses by increasing the activation and recruitment of effector T cells (1, 21).

Identification of chemokines as the primary mediators of leukocyte recruitment toward sites of infection and tumors

TABLE 1. Reduced viral titers within the brain correlate with increased NK infiltration

Virus	Day post-infection	Titer (log_{10} PFU/g of tissue)	Total NK (%)
Alb275	2	4.6 ± 0.4	$9.0 \pm 0.4 \times 10^4$ (26)
	5	6.7 ± 0.2	$7.0 \pm 1 \times 10^3$ (5)
	8	6.5 ± 0.3	ND
	12	ND	ND
Alb275 + anti-CXCL10	2	6.1 ± 0.2[c]	$4.0 \pm 0.2 \times 10^4$ (14)[a]
	5	6.5 ± 0.4	$2.0 \pm 0.1 \times 10^3$ (2)[a]
Alb274	2	3.6 ± 0.2[d]	$2.1 \pm 0.1 \times 10^5$ (40)[b]
	5	4.9 ± 0.7[d]	$8.0 \pm 0.4 \times 10^4$ (27)[b]
	8	4.8 ± 0.3[d]	$9.0 \pm 0.2 \times 10^3$ (17)
	12	6.4 ± 0.2	ND
Alb274 + anti-CXCL10	2	5.8 ± 0.4[c]	$3.0 \pm 0.1 \times 10^4$ (19)[a]
	5	6.0 ± 0.2[c]	$2.0 \pm 0.4 \times 10^3$ (17)[a]
Alb274 + anti-NK1.1	2	5.3 ± 0.4[e]	$2.5 \pm 0.1 \times 10^3$ (12)[a]
	5	5.7 ± 0.4[e]	$2.0 \pm 0.2 \times 10^3$ (23)[a]
Alb274 + anti-IFN-γ	8	5.8 ± 0.1[f]	$5.2 \pm 0.2 \times 10^3$ (8)

[a] Data are presented as the average ± SEM. $P \leq 0.02$; reduced NK cell infiltration following treatment with either neutralizing anti-CXCL10 or anti-NK1.1 antibodies. Data represent results from three experiments with at least three mice per group.

[b] $P \leq 0.0001$; enhanced NK cell infiltration following Alb274 infection compared to infection with Alb275. Data represent results from five experiments with three mice per group.

[c] $P \leq 0.006$. Increased recovery of replicating virus from the CNS following treatment with neutralizing anti-CXCL10 antibodies. Data represent results from three experiments with three mice per group.

[d] $P \leq 0.001$. Reduced viral titers following Alb274 infection compared to infection with Alb275. Data represent results from five experiments with three mice per group.

[e] $P \leq 0.02$. Increased viral titers following treatment with anti-NK1.1 antibodies compared to mice infected with Alb274. Data represent results from two separate experiments with three mice per group.

[f] $P \leq 0.002$. Increased viral titers following treatment with neutralizing anti-IFN-γ antibodies compared to Alb274-infected mice. Data represent results from two separate experiments with four mice per group.

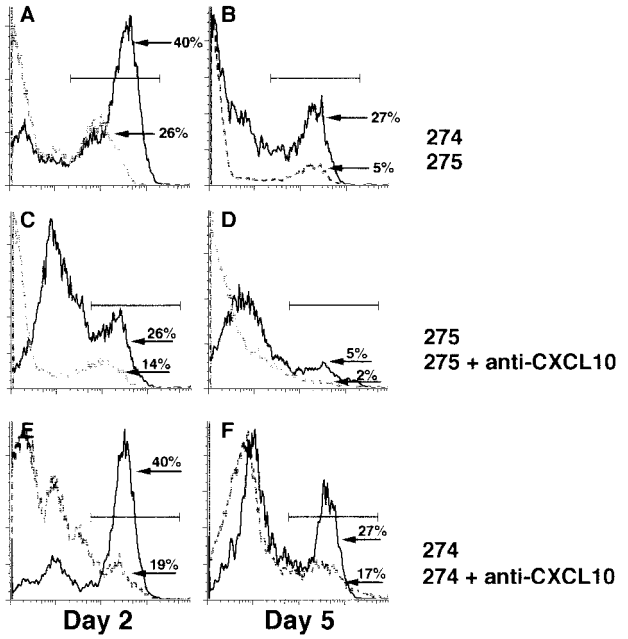

FIG. 5. (A and B) Analysis of NK cell infiltration following Alb274 and Alb275 infection. Total mononuclear cells were isolated from the CNS at 2 and 5 days postinfection and stained with fluorescein isothiocyanate-conjugated anti-NK1.1. Representative histograms show the percentages of NK1.1-positive cells present in the CNS of Alb274- and Alb275-infected mice. Alb274 infection resulted in a significant increase in NK cell infiltration at both 2 and 5 days postinfection ($P \leq 0.0001$). Data presented represent a total of five separate experiments with at least three mice per group; $n = 15$. (C, D, E, and F) NK cell infiltration following anti-CXCL10 treatment. Anti-CXCL10 treatment at −1, 1, and 3 days postinfection resulted in a dramatic decrease in NK cell infiltration following either Alb275 (C and D) or Alb274 (E and F) infection at both 2 and 5 days postinfection ($P \leq 0.02$). Data presented are representative of the results obtained from three separate experiments with three mice per experiment; $n = 9$.

indicated that viral expression of select CXC chemokines would also enhance antiviral immunity and reduce tumor sizes. Indeed, recent reports have demonstrated a critical role for CXCL10 in directing effector T-cell migration towards tumor growth, which then facilitates regression of established tumors (31). Moreover, recent studies have demonstrated an important role for CXCL10 in participating in innate defense against vaccinia virus infection by recruiting and activating NK cells (24). These results clearly indicate that CXCL10 participates in both innate and adaptive host defense mechanisms by contributing to cell migration and activation.

Our studies further attest to the ability of CXCL10 to contribute to innate immune response to viral infection. Importantly, the results presented define a pivotal role for CXCL10 in evoking innate immune responses within the CNS in response to viral infection. Intracerebral infection of *RAG1*$^{-/-}$ mice with recombinant MHV expressing CXCL10 resulted in a dramatic reduction in both mortality and morbidity that correlated with reduced viral replication within the CNS. Within the context of this model system, CXCL10 mediated its protective effect by coordinating the infiltration and activation of NK cells into the brain, as anti-CXCL10 treatment abolished NK cell-mediated protection. Importantly, our data indicate that endogenous expression of CXCL10 within the brains of wild-type-MHV-infected *RAG1*$^{-/-}$ mice is also important in defense, as anti-CXCL10 treatment resulted in increased viral titers accompanied by reduced infiltration of NK cells. These findings are novel in that no chemokine has yet been shown to exert a clearly defined role in coordinating an innate immune response following viral infection of the CNS. In addition, these results clearly indicate that NK cells can exert an antiviral protective effect within the CNS.

Previous studies have demonstrated the recruitment and activation of NK cells following infection with a wide range of viruses (4). However, not all viral infections are susceptible to NK-mediated clearance, and susceptibility depends upon the effector mechanisms induced. For example, the induction of both cytotoxicity and IFN-γ production by NK cells following murine cytomegalovirus and influenza virus infection results in reduced virally induced disease and enhanced survival (27, 29). In contrast, the absence of IFN-γ production by NK cells correlates with the absence of an effective innate response to lymphocytic choriomeningitis virus infection (37). Moreover, the organs targeted by viral infection can also influence the participation of NK cells. Indeed, Tay et al. (35) demonstrated that the NK response to murine cytomegalovirus is perforin dependent within the spleen, whereas production of IFN-γ is required for viral clearance from the liver. These results indicate that the importance of the NK cell response to viral

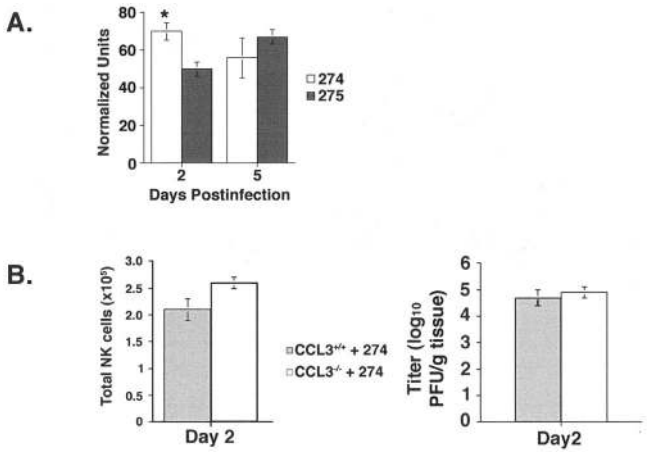

FIG. 6. *CCL3* gene expression within the CNS following Alb274 and Alb275 infection. (A) Densitometric analysis of *CCL3* mRNA transcripts obtained from the scanned autoradiograph of an RNase protection assay. Transcripts for CCL3 were detected following both infections at all time points analyzed. *CCL3* transcripts were significantly increased at day 2 postinfection following Alb274 infection compared to Alb275-infected mice ($P \leq 0.05$). (B) NK cell infiltration and viral titers in $CCL3^{-/-}$ mice. Alb274 infection of $CCL3^{-/-}$ mice resulted in equivalent NK cell infiltration compared to Alb274-infected wild-type C57BL/6 mice at 2 days postinfection, and this correlated with no observable difference in the level of viral replication between wild-type and $CCL3^{-/-}$ mice. All experiments were performed in duplicate with a minimum of three mice per experiment; $n = 6$.

infection can depend upon multiple factors, including the tissue infected as well as the effector mechanisms induced.

The significance of NK cells in controlling MHV replication within the CNS of $RAG1^{-/-}$ mice was confirmed by the dramatic increase in mortality following the administration of anti-NK1.1 antibodies. Similar to treatment with anti-CXCL10 antibodies, antibody-mediated targeting of NK cells resulted in increased viral replication within the CNS of MHV-infected $RAG1^{-/-}$ mice, suggesting that NK cell recruitment to the CNS is critical in controlling viral replication prior to the recruitment of the adaptive immune response. Moreover, the enhanced accumulation of NK cells within the CNS following Alb274 infection directly correlated with a dramatic increase in IFN-γ production, suggesting that secretion of cytokines may be a primary mechanism for controlling viral replication within the CNS. Indeed, neutralization of IFN-γ with neutralizing monoclonal antibodies resulted in increased mortality and reduced viral clearance compared to Alb274-infected mice. These results suggest that virus-encoded CXCL10 is able to enhance the production of IFN-γ by NK cells within the CNS. Similarly, Mahalingam et al. (24) demonstrated the importance of CXCL10-induced NK production of IFN-γ within the ovaries and lungs following vaccinia virus infection. Neutralization of IFN-γ in mice infected with a recombinant vaccinia virus encoding CXCL10 resulted in a dramatic increase in viral titers, suggesting that clearance of virus was dependent upon interferon production. Similarly, the data presented indicate that within the CNS, IFN-γ production by NK cells is critical in the control of MHV replication, which is consistent with previous studies (15, 30).

In summary, our results indicate a critical role for CXCL10 in the protection of $RAG1^{-/-}$ mice from virus-induced CNS disease. Combined with our previous studies identifying this chemokine as a potent T-cell chemoattractant and mediator of the protective adaptive immune response, our results indicate that early expression of CXCL10 is required for the recruitment and activation of NK cells. NK cells are able to protect the host by controlling viral replication, presumably until antigen-specific T cells arrive. Therefore, our findings further delineate the functional contributions of CXCL10 to host defense and clearly indicate an important signaling link between innate and adaptive immunity following viral infection of the CNS.

ACKNOWLEDGMENTS

This work was supported by National Institutes of Health grants NS37336 and NS41429 and National Multiple Sclerosis Society grant R63278-A-3 (T.E.L.) and by National Institutes of Health grant AI 39544 (P.S.M.).

We are grateful to Cheri Koetzner for assisting with the viral growth comparison and Lili Kuo for the labeling of viral RNA. We thank the Molecular Genetics Core Facility of the Wadsworth Center for synthesis of oligonucleotides and automated DNA sequencing.

REFERENCES

1. **Addison, C., T. Braciak, R. Ralston, W. Muller, J. Gauldie, and F. Graham.** 1995. Intratumoral injection of an adenovirus expressing IL-2 induces regression and immunity in a murine breast cancer model. Proc. Natl. Acad. Sci. USA **92:**8522–8526.
2. **Arai, K., Z. X. Liu, T. E. Lane, and G. Dennert.** 2002. IP-10 and Mig facilitate accumulation of T cells in the virus-infected liver. Cell. Immunol. **219:**48–56.
3. **Arenberg, D. A., S. L. Kunkel, P. J. Polverini, S. B. Morris, M. D. Burdick, M. C. Glass, D. T. Taub, M. D. Iannettoni, R. I. Whyte, and R. M. Strieter.** 1996. Interferon-gamma-inducible protein 10 (IP-10) is an angiostatic factor that inhibits human non-small cell lung cancer (NSCLC) tumorigenesis and spontaneous metastases. J. Exp. Med. **184:**981–992.
4. **Biron, C. A., K. B. Nguyen, G. C. Pien, L. P. Cousens, and T. P. Salazar-Mather.** 1999. Natural killer cells in antiviral defense. Annu. Rev. Immunol. **17:**189–220.
5. **Bonecchi, R. G., G. Bianchi., P. P. Bordignon, D. D. Ambrosio, R. Lang, A. Borsatti, S. Sozzani, P. Allavena, A. Gray, A. Mantovani, and F. Sinigaglia.** 1998. Differential expression of chemokine receptors and chemotactic responsiveness of type 1 T helper cells (Th1s) and Th2s. J. Exp. Med. **187:** 129–134.
6. **Cole, A. M., T. Ganz, A. M. Liese, M. D. Burdick, L. Liu, and R. M. Strieter.** 2001. IFN-inducible ELR-CXC chemokines display defensin-like antimicrobial activity. J. Immunol. **167:**623–627.
7. **Cook, D. N., M. A. Beck, T. M. Coffman, S. L. Kirby, J. F. Sheridan, I. B. Pragnell, and O. Smithies.** 1995. Requirement of MIP-1 alpha for an inflammatory response to viral infection. Science **269:**1583–1585.
8. **Dufour, J. H., M. Dziejman, M. T. Liu, J. H. Leung, T. E. Lane, and A. D. Luster.** 2002. IFN-γ-inducible protein 10 (IP-10; CXCL10)-deficient mice reveal a role for immunoprecipitation-10 in effector T-cell generation and trafficking. J. Immunol. **168:**3195–3204.
9. **Fischer, F., C. F. Stegen, C. A. Koetzner, and P. A. Masters.** 1997. Analysis of a recombinant mouse hepatitis virus expressing a foreign gene reveals a novel aspect of coronavirus transcription. J. Virol. **71:**5148–5160.
10. **Jackson, R. J., A. J. Ramsay, C. D. Christensen, S. Beaton, D. F. Hall, and I. A. Ramshaw.** 2001. Expression of mouse interleukin-4 by a recombinant ectromelia virus suppresses cytolytic lymphocyte responses and overcomes genetic resistance to mousepox. J. Virol. **75:**1205–1210.
11. **Kakimi, K., T. E. Lane, S. Wieland, V. C. Asensio, I. L. Campbell, F. V. Chisari, and L. G. Guidotti.** 2001. Blocking chemokine responsive to gamma-2/interferon (IFN)-gamma inducible protein and monokine induced by IFN-gamma activity in vivo reduces the pathogenetic but not the antiviral potential of hepatitis B virus-specific cytotoxic T lymphocytes. J. Exp. Med. **194:**163–172.
12. **Koetzner, C. A., M. M. Parker, C. S. Ricard, L. S. Sturman, and P. S. Masters.** 1992. Repair and mutagenesis of the genome of a deletion mutant of the coronavirus mouse hepatitis virus by targeted RNA recombination. J. Virol. **66:**1841–1848.
13. **Kuo, L., G. J. Godeke, M. J. B. Raamsman, P. S. Masters, and P. J. M. Rottier.** 2000. Retargeting of coronavirus by substitution of the spike glycoprotein ectodomain: crossing the host cell species barrier. J. Virol. **74:**1393–1406.
14. **Lai, M. M. C., and D. Cavanagh.** 1997. The molecular biology of coronaviruses. Adv. Virus Res. **48:**1–100.

15. **Lane, T. E., A. D. Paoletti, and M. J. Buchmeier.** 1997. Disassociation between the in vitro and in vivo effects of nitric oxide on a neurotropic murine coronavirus. J. Virol. **71:**2202–2210.
16. **Lane, T. E., and M. J. Buchmeier.** 1997. Murine coronavirus infection: a paradigm for virus induced demyelinating disease. Trends Microbiol. **5:**9–14.
17. **Lane, T. E., M. T. Liu, B. P. Chen, V. C. Asensio, R. M. Samawi, A. D. Paoletti, I. L. Campbell, S. L. Kunkel, H. S. Fox, and M. J. Buchmeier.** 2000. A central role for $CD4^+$ T cells and RANTES in virus-induced central nervous system inflammation and demyelination. J. Virol. **74:**1415–1424.
18. **Lane, T. E., V. C. Asensio, N. Yu, A. D. Paoletti, I. L. Campbell, and M. J. Buchmeier.** 1998. Dynamic regulation of alpha and beta chemokine expression in the central nervous system during mouse hepatitis virus-induced demyelinating disease. J. Immunol. **160:**970–978.
19. **Liu, M. T., B. P. Chen, P. Oertel, M. J. Buchmeier, D. Armstrong, T. A. Hamilton, and T. E. Lane.** 2000. Cutting edge: the T-cell chemoattractant IFN-inducible protein 10 is essential in host defense against viral-induced neurologic disease. J. Immunol. **165:**2327–2330.
20. **Liu, M. T., H. S. Keirstead, and T. E. Lane.** 2001. Neutralization of the chemokine CXCL10 reduces inflammatory cell invasion and demyelination and improves neurological function in a viral model of multiple sclerosis. J. Immunol. **167:**4091–4097.
21. **Liu, Y., H. Huang, A. Saxena, and J. Xiang.** 2001. Intratumoral coinjection of two adenoviral vectors expressing functional interleukin-18 and inducible protein-10, respectively, synergizes to facilitate regression of established tumors. Cancer Gene Ther. **9:**533–542.
22. **Loetscher, M., B. Gerber, P. Loetscher, S. A. Jones, L. Piali, I. C. Lewis, M. Baggiolini, and B. Moser.** 1996. Chemokine receptor specific for IP-10 and Mig: structure, function, and expression in activated T-lymphocytes. J. Exp. Med. **184:**963–969.
23. **Maghazachi, A. A., B. S. Skalhegg, B. Rolstad, and A. Al-Aoukaty.** 1997. Interferon-inducible protein-10 and lymphotactin induce the chemotaxis and mobilization of intracellular calcium in natural killer cells through pertussis toxin-sensitive and -insensitive heterotrimeric G-proteins. FASEB J. **11:**765–774.
24. **Mahalingam, S., J. M. Farber, and G. Karupiah.** 1999. The interferon-inducible chemokines MuMig and Crg-2 exhibit antiviral activity in vivo. J. Virol. **73:**1479–1491.
25. **Masters, P.** 1999. Reverse genetics of the largest RNA viruses. Adv. Virus Res. **53:**245–264.
26. **Masters, P. S., C. A. Koetzner, C. A. Kerr, and Y. Heo.** 1994. Optimization of targeted RNA recombination and mapping of a novel nucleocapsid gene mutation in the coronavirus mouse hepatitis virus. J. Virol. **68:**328–337.
27. **Monteiro, J. M., C. Harvey, and G. Trinchieri.** 1998. Role of interleukin-12 in primary influenza virus infection. J. Virol. **72:**4825–4831.
28. **Ontiveros, E., L. Kuo, P. S. Masters, and S. Perlman.** 2001. Inactivation of expression of gene 4 of mouse hepatitis virus strain JHM does not affect virulence in the murine CNS. Virology **289:**230–238.
29. **Orange, J. S., B. Wang, C. Terhorst, and C. A. Biron.** 1995. Requirement for natural killer cell-produced interferon-γ in defense against murine cytomegalovirus infection and enhancement of this defense pathway by interleukin 12 administration. J. Exp. Med. **182:**1045–1056.
30. **Parra, B., D. R. Hinton, N. W. Marten, C. C. Bergmann, M. T. Lin, C. S. Yang, and S. A. Stohlman.** 1999. IFN-gamma is required for viral clearance from central nervous system oligodendroglia. J. Immunol. **162:**1641–1647.
31. **Putzer, B., H. Mary, W. Muller, P. Emtage, J. Gauldie, and F. Graham.** 1997. Interleukin 12 and B7–1 costimulatory molecule expressed by an adenovirus vector act synergistically to fascilitate tumor regression. Proc. Natl. Acad. Sci. USA **94:**1088–1094.
32. **Ramshaw, I. A., A. J. Ramsay, G. Karupiah, M. S. Rolph, S. Mahalingam, and J. C. Ruby.** 1997. Cytokines and immunity to viral infections. Immunol. Rev. **159:**119–135.
33. **Salazar-Mather, T. P., J. S. Orange, and C. A. Biron.** 2002. Early murine cytomegalovirus (murine cytomegalovirus) infection induces liver natural killer (NK) cell inflammation and protection through macrophage inflammatory protein 1α (MIP-1α)-dependent pathways. J. Exp. Med. **187:**1–14.
34. **Stohlman, S. A., P. R. Brayton, R. C. Harmon, D. Stevenson, R. G. Ganges, and G. K. Matsushima.** 1983. Natural killer cell activity during mouse hepatitis virus infection: response in the absence of interferon. Int. J. Cancer **31:**309–314.
35. **Tay, C. H., and R. M. Welsh.** 1997. Distinct organ-dependent mechanisms for the control of murine cytomegalovirus infection by natural killer cells. J. Virol. **71:**267–275.
36. **Weiss, S. R., P. W. Zoltick, and J. L. Leibowitz.** 1993. The ns 4 gene of mouse hepatitis virus (MHV), strain A59 contains two ORFs and thus differs from ns 4 of the JHM and S strains. Arch. Virol. **129:**301–309.
37. **Welsh, R. M.** 1978. Cytotoxic cells induced during lymphocytic choriomeningitis virus infection of mice. I. Characterization of natural killer cell induction. J. Exp. Med. **148:**163–181.
38. **Yokomori, K., and M. M. C. Lai.** 1991. Mouse hepatitis virus S RNA sequence reveals that nonstructural proteins ns4 and ns5a are not essential for murine coronavirus replication. J. Virol. **65:**5605–5608.